Ultrasound can Modulate Neuronal Development: Impact on Neurite Growth and Cell Body Morphology

ARTICLE *in* ULTRASOUND IN MEDICINE & BIOLOGY · FEBRUARY 2013

Impact Factor: 2.21 · DOI: 10.1016/j.ultrasmedbio.2012.12.003 · Source: PubMed

4 AUTHORS, INCLUDING:

Yaxin Hu
The University of Hong Kong
6 PUBLICATIONS **29** CITATIONS
SEE PROFILE

Jennifer Wan
The University of Hong Kong
85 PUBLICATIONS **1,077** CITATIONS
SEE PROFILE

Ultrasound in Med. & Biol., Vol. 39, No. 5, pp. 915–925, 2013

0301-5629/$ - see front matter

http://dx.doi.org/10.1016/j.ultrasmedbio.2012.12.003

● *Original Contribution*

ULTRASOUND CAN MODULATE NEURONAL DEVELOPMENT: IMPACT ON NEURITE GROWTH AND CELL BODY MORPHOLOGY

YAXIN HU,* WENJING ZHONG,* JENNIFER M. F. WAN,† and ALFRED C. H. YU*

*Medical Engineering Program, The University of Hong Kong, Pokfulam, Hong Kong SAR; and †School of Biological Sciences, The University of Hong Kong, Pokfulam, Hong Kong SAR

(*Received* 4 *July* 2012; *revised* 6 *December* 2012; *in final form* 8 *December* 2012)

Abstract—Neuronal development is known to be a dynamic process that can be modulated by presenting guidance cues to neuronal cells. We show that ultrasound, when applied at pulsed settings and with intensities slightly greater than clinical diagnosis levels, can potentially act as a repulsive cue for modulating neuronal growth dynamics. Using differentiated Neuro-2a cells as the model, we have examined *in vitro* how neuronal development can change during and after exposure to 1-MHz ultrasound for different acoustic settings. Neurite retraction and cell body shrinkage were found in neuronal cells over a 10-min exposure period with 1.168 W/cm^2 spatial-peak, time-averaged intensity (based on 0.84 MPa peak acoustic pressure, 100-cycle pulse duration, and 500-Hz pulse repetition frequency). These effects were found to result in instances of neuronal cell body displacement. The extent of the effects was dependent on acoustic intensity, with peak acoustic pressure being a more important contributing factor compared with pulse duration. The morphological changes were found to be non-destructive, in that post-exposure neurite outgrowth and neuritogenesis were respectively observed in neurite-bearing and neurite-less neuronal cells. Our results also showed that mechanotransduction might be involved in mediating ultrasound-neuron interactions, as the morphological changes were suppressed if stretch-activated ion channels were blocked or if calcium messenger ions were chelated. Overall, these findings suggest that ultrasound can potentially influence how neuronal cells develop through modifying their cytomechanical characteristics. (E-mail: alfred.yu@hku.hk and jmfwan@hku.hk) **© 2013 World Federation for Ultrasound in Medicine & Biology.**

Key Words: **Ultrasound, Neuronal development, Repulsive cue, Neurite retraction, Cell body shrinkage, Cell body displacement, Mechanotransduction.**

INTRODUCTION

Neuronal development is known to be a highly dynamic course of action that involves establishing an interconnected network of neurons to form the structural basis for functional neuronal circuits (van Ooyen 2011). A core event in facilitating such development is the outgrowth of neurite branches (or processes) from a post-mitotic neuron's cell body (also known as soma) where the nucleus and various organelles are located (Arimura and Kaibuchi 2007; Da Silva and Dotti 2002). It is well recognized that the development of neuronal cells is intrinsically regulated by various cytoplasmic signaling cascades (Goldberg 2004; Rossi et al. 2007) and cytomechanical factors (Ayali 2010; Suter and Miller 2011). To facilitate their growth, developing neurons and their neurites would continually probe their surrounding environment to identify local conditions that favor their development and avoid unfavorable ones (Franze and Guck 2010). As such, by presenting external guidance cues to the extracellular environment, neuronal development can potentially be modulated.

A few types of extracellular cues have been determined as being capable of regulating the growth of developing neurons and in turn modulating the morphogenesis of neuronal networks. One of them is the biochemical approach whereby molecular gradients of netrin, ephrin or similar signaling proteins are introduced to the extracellular environment to modify neuronal growth dynamics (Guan and Rao 2003; Song and Poo 2001). Another approach is to introduce patterned topologies on the attachment substrate to guide neuronal navigation (Hoffman-Kim et al. 2010). Physical cues have also been considered, and they involve the application of electrical (Ming et al. 2001), optical (Ehrlicher et al. 2002) or mechanical forces (Franze et al. 2009; Smith 2009) to

Address correspondence to: Alfred C. H. Yu, The University of Hong Kong, Pokfulam Road, Hong Kong. E-mail: alfred.yu@hku.hk and Jennifer M. F. Wan, The University of Hong Kong, Pokfulam Road, Hong Kong. E-mail: jmfwan@hku.hk

stimulate neurite extension or retraction. From an application standpoint, these types of cues can significantly benefit neural tissue engineering under cell culture settings (Norman et al. 2008; Schmidt and Leach 2003). Nevertheless, their direct application to neural treatments (*e.g.*, as a cure for neuronal development disorders) is perhaps not a trivial task because targeted, non-invasive delivery of these cues *in vivo* might not be straightforward, especially for topological cues that are delivered based on grafting mechanisms.

In this work, we seek to investigate whether and how ultrasound can be exploited as another type of guidance cue for neuronal development. We hypothesize that ultrasound, when applied at low intensity and pulsed settings, can possibly serve as a physical cue that operates under principles similar to those based on mechanical force stimulation (Franze et al. 2009; Smith 2009). This hypothesis is formed on the basis that ultrasound, as an acoustic form of radiation, is known to be able to produce mechanical bioeffects on living cells without causing temperature elevation (Ahmadi et al. 2012; Dalecki 2004). The technical advantage of using ultrasound is that it can be delivered remotely to the target area in a non-invasive manner using well-established beam focusing principles. Therefore, ultrasound might have potential in being applied clinically to modulate neuronal development. It is worth noting that the neuromodulation potential of ultrasound has been explored recently in the context of peripheral nerve regeneration (Chang and Hsu 2004; Chen et al. 2010; Crisci and Ferreira 2002) and functional neuronal circuit excitation (Bystritsky et al. 2011; Tufail et al. 2010, 2011; Tyler et al. 2008). Our investigation reported here can serve to complement these ongoing efforts by providing novel insight on ultrasound-neuron interactions from a neuronal development perspective and at a single-cell level.

The focus of this study is on demonstrating that ultrasound can be a repulsive cue for modulating neuronal growth dynamics *in vitro*. In particular, it will be shown that ultrasound may induce various morphological changes in neuronal cells and in turn modify their physical positioning and developmental behavior. We also seek to provide evidence on the cellular mechanism involved in this process. Data will be presented to show that stretch-activated ion channels and calcium ion (Ca^{2+}) signaling are playing a direct role in a neuronal cell's ability to sense pulsed ultrasound stimulation.

MATERIALS AND METHODS

Exposure platform components

Ultrasound transmission device. A customized experimental platform has been developed for this work. As illustrated in Figure 1, the platform sends ultrasound pulses through a piston transducer with a center frequency of 1 MHz and diameter of 25.4 mm (Wuxi Beisheng Technology, Wuxi, Jiangsu, China). The pulse shape was defined using an arbitrary waveform generator (33120A; Agilent Technologies, Santa Clara, CA, USA), and a broadband power amplifier (2100L; Electronics and Innovation, Rochester, NY, USA) was used to boost the electrical signal that drives the ultrasound transducer. To collimate ultrasound energy to the microscope's field of view (*i.e.*, center of the xy-plane), the transducer was mounted onto a custom-made, water-coupled hollow cone waveguide (79 mm total cone height; acrylic casing) with a detachable tip (upper 9 mm of the cone height) that was removed following physical alignment (*i.e.*, after positioning the tip in contact with the center of the field of view). Note that the transducer-waveguide block was clamped to a retort stand. It was elevationally angled at 45 degrees (with respect to the z-axis) using an angle plate, and its rotational angle about the z-axis was 42 degrees (calibrated *in situ*; to be discussed in the Acoustic Field Calibration subsection).

Sample holder. A 100-mm–diameter polystyrene dish (430167; Corning Life Sciences, Tewksbury, MA, USA) was used as the host substrate for neuronal cells. Its plate layer was 0.9 mm thick, and it was slightly elevated by 0.5 mm with respect to the bottom of the cylindrical side casing. During operation, the cell dish was placed upon a larger polystyrene container that was filled with 37°C degassed water (0.8 mm thick; 20 mm high; 180 × 112 mm base dimensions). In turn (Fig. 1, insert), this resulted in the formation of a 2.2-mm–thick multi-layer base (*i.e.*, a water layer sandwiched between two polystyrene layers). Such a configuration was used so that, as confirmed by our hydrophone measurements (see subsection on Acoustic Field Calibration), incident ultrasound pulses impinging on the cell dish at a 45-degree angle would reflect out at a distance away from the incidence point (as an angled reflection from the bottom air interface), and in turn strong *in situ* reflections would be avoided. This helped to maintain acoustic field homogeneity over the microscope's field of view.

Imaging of neuronal cells. To facilitate real-time imaging of neuronal development dynamics during and after ultrasound exposure, our experimental platform was equipped with an inverted phase contrast microscope (Leica DM IL; Leica Microsystems, Wetzlar, Germany) carrying a 10× objective (numerical aperture: 0.20). A color video camera (TK-C9510E; JVC, Yokohoma, Japan) was used to acquire images from the microscope at a frame rate of up to 25 frames per second (fps). The camera images were 720 × 576 pixels, and the field-of-view was 650 × 500 μm (*i.e.*, pixel dimension: 0.90 × 0.87 μm). In each experiment trial, image frames

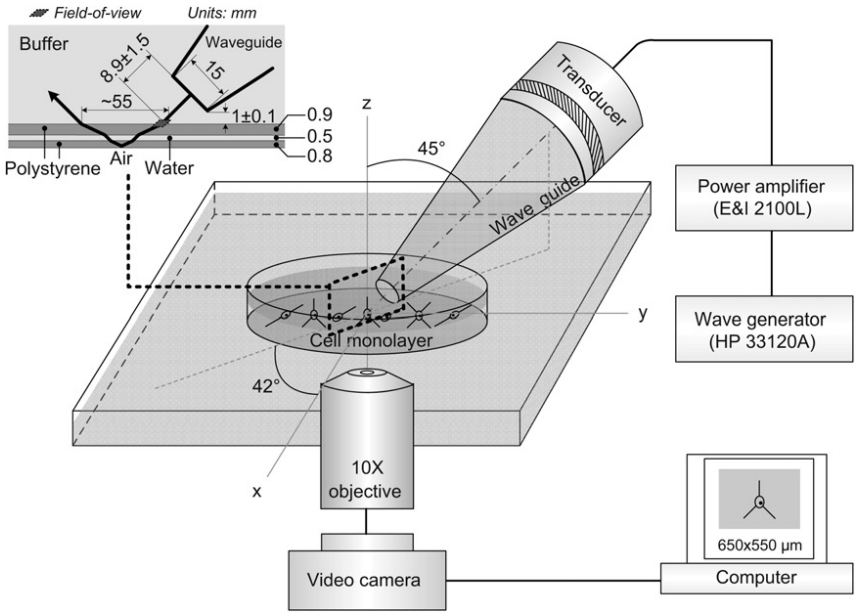

Fig. 1. Illustration of the experimental platform. The ultrasound transducer is positioned at 79 mm away from the microscope's field of view. The figure insert shows a schematic diagram of the sample holder composition, along with the acoustic propagation path and physical dimensions. Real-time monitoring of the developmental dynamics of neuronal cells in response to ultrasound modulation was performed using the phase contrast microscope and the video camera. The field of view is 650 × 500 μm (inverted view).

were recorded over the time window that spans from the start of exposure to 100 min after the end of exposure, and they were streamed in real time to a computer workstation. This method allowed us to conduct offline image analysis to determine how neuronal cells change their developmental dynamics in response to ultrasound.

Acoustic field calibration

Hydrophone measurement setup. To characterize the acoustic field profile generated by our ultrasound transmission setup, we have performed hydrophone measurements of both free-field pressure and *in situ*–reflected pressure. A needle hydrophone was used to take these measurements (HNR-0500, ONDA Corporation, Sunnyvale, CA, USA), and its positioning was controlled by a three-axis scan stage (ASTS-01; ONDA Corporation). For the free-field measurements (performed inside a 37°C water bath), the transducer-waveguide block (with tip detached) was first aligned in parallel with the hydrophone tip, and planar scans were made at a 45-degree elevational angle (Fig. 2a)—that is, in line with the actual transducer angle during operation. *In situ* reflected pressure was measured with the hydrophone tip facing the polystyrene dish surface that corresponds to the $z = 0$ mm plane (Fig. 2b).

Free-field pressure mapping. For a pulse duration (PD) of 100 cycles, Figure 2a shows the corresponding hydrophone waveform detected at the pressure field's spatial peak, which is assumed to geometrically correspond to the apex of the cone-shaped waveguide. As can be noted, the incident pulses generally maintained their typical multi-cycle sinusoidal pattern at the spatial peak. Indeed, the xy-plane free-field map of peak acoustic rarefactional pressure ($P_{\max}$) shows that the acoustic field produced by our ultrasound transmission setup was rather homogeneous over the microscope's field of view (650 × 500 μm; demarcated by the dashed window in the enlarged version of the xy-plane pressure map).

Three different $P_{\max}$ levels were used in this study: 0.13, 0.40, and 0.84 MPa (achieved by adjusting the input electrical voltage on the waveform generator). With these values, the spatial-peak, time-averaged (SPTA) intensity (I_{SPTA}) was estimated for different PDs (20 or 100 cycles) and pulse repetition frequency (PRF) values (500 or 2500 Hz). The I_{SPTA} range used in our experiments was calculated to be between 0.028–1.168 W/cm^2 according to the following well-established formula that assumes plane-wave propagation (Halliwell 2010):

$$I_{SPTA} = \frac{|P_{\max}|^2}{2\rho c}\delta \quad \text{for} \quad \delta = \frac{N_{cycle}}{f_o} f_{PRF}.$$

where ρ and c are the density and acoustic speed in 37°C water (993 kg/m^3 and 1520 m/s), respectively; also, δ denotes duty cycle (1% or 5% in this work), and it can be estimated from finding the product between PD and PRF (N_{cycle} and f_o respectively denote number of cycles per pulse and ultrasound frequency).

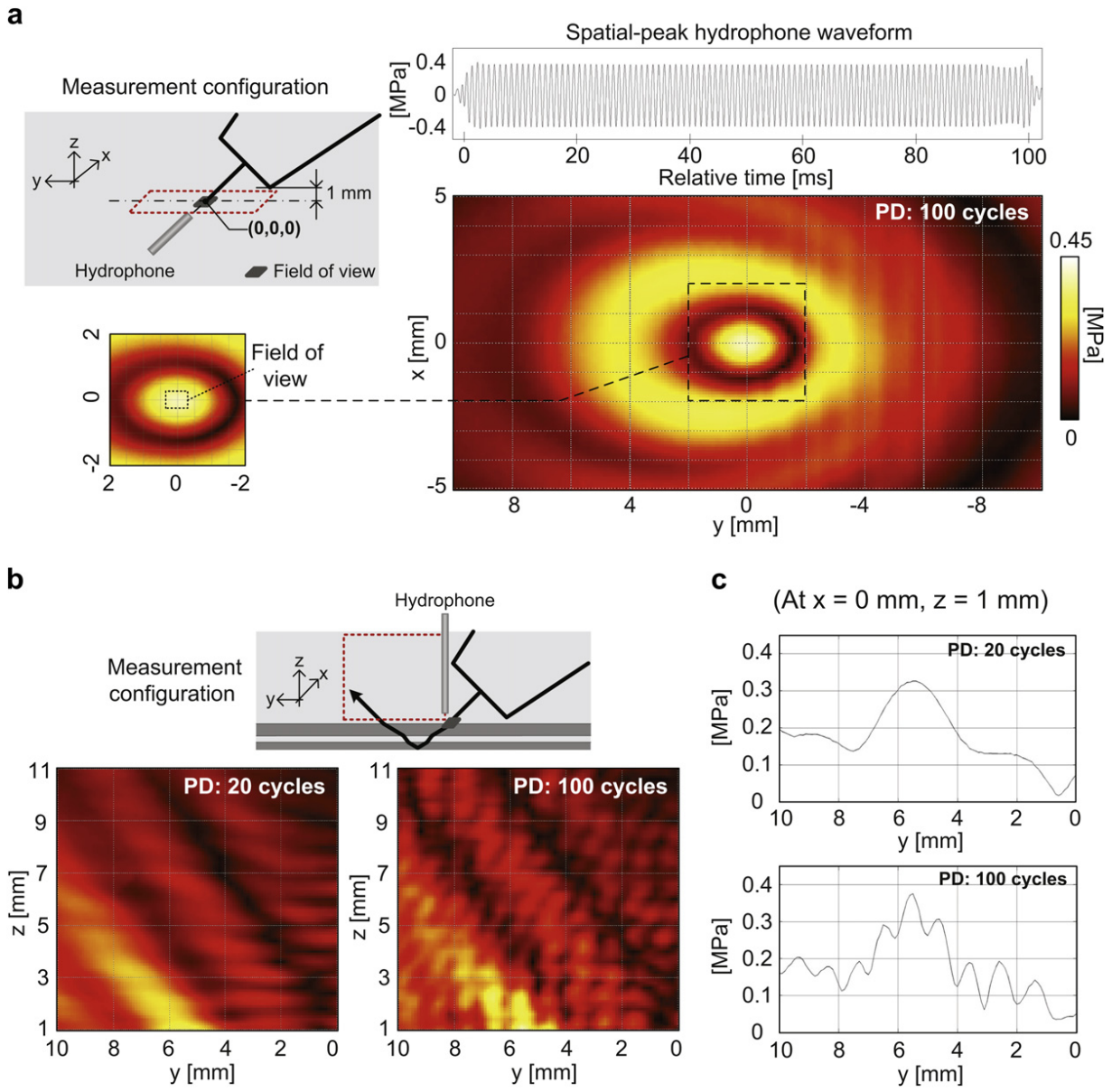

Fig. 2. Acoustic pressure field maps of our ultrasound exposure platform. Results are provided for an ultrasound frequency of 1 MHz and a free-field peak negative pressure of 0.40 MPa. Two different measurement configurations were used: (a) free-field measurements (showing the spatial-peak acoustic pressure waveform and the xy-plane peak acoustic pressure map for the 100-cycle PD); (b) *in situ* reflection measurements showing the reflected pressure map along the yz-plane for both 20-cycle and 100-cycle PDs. (c) Plots of the reflected pressure as a function of y-axis position are shown for the $z = 1$ mm plane (the measurement plane closest to the dish surface).

In situ *reflected pressure mapping*. As an insight into the *in situ* acoustic field conditions, Figure 2b shows yz-plane maps of the reflected pressure for PD of 20 and 100 cycles (the hydrophone tip was positioned at least 1 mm away from the dish surface to avoid contact). For both PDs, there is a high reflected pressure zone in the form of an angled z-axis projection stemming from the 55-mm point on the y-axis. It corresponds to the main path of acoustic reflection returning from the air interface at the platform base (Fig. 1, insert). In contrast, low reflected pressure was observed near the incidence point at the y-axis origin close to the dish surface (*i.e.*, bottom-right corner in the pressure maps of Fig. 2b) where the microscope's field of view was located.

As further analysis of the *in situ* acoustic field near the dish surface, Figure 2c shows the reflected pressure plots along the y-axis at $z = 1$ mm. Note that, from these plots, the reflected pressure near the incidence point can be approximated from the values over the y-axis range of 0–1 mm, within the dimensions of the microscope's

field of view. This pressure was less than 0.07 MPa for both 20- and 100-cycle PDs, and it was significantly lower than the incident free-field pressure (0.40 MPa). Indeed, the reflectance (*i.e.*, squared ratio between reflected and incident pressures) was calculated to be 3% in this case, which signifies that 97% of incident wave energy was transmitted into the platform base at the incidence point.

Another trend worth noting from the *in situ* hydrophone measurements is that standing wave patterns in the form of spatial rippling were present in the reflected pressure profiles. Indeed, for the case with 100-cycle PD, standing waves appeared along both the y- and z-axes (antinodes were spaced apart by ∼1 mm, which corresponds to the wavelength along each axis for a 45-degree incidence angle). The physical origin of these standing waves can be attributed to the reflective air interfaces at the cell dish's cylindrical side and the buffer medium's top surface. Fortunately, as indicated in Figure 2c, this pressure-rippling phenomenon was apparent only away from the incidence point. As such, the effect of standing waves on the *in situ* pressure field over the microscope's field of view can be considered insignificant.

Estimation of ultrasound propagation direction. To determine the *in situ* ultrasound propagation direction within the microscope's field of view (*i.e.*, on the xy-plane), we have conducted a calibration test in which micro-beads with a diameter of 6 μm diameter (345249; BD Biosciences, San Jose, CA, USA) were placed in the polystyrene dish, and their displacement direction was observed in the presence of ultrasound exposure, which would exert radiation force along its path. All micro-beads were found to displace uniformly from the bottom-left to the upper-right section of the field of view. Offline analysis of microscope video frames using an in-house Matlab script (version 2012a; Mathworks, Natick, MA, USA) showed that the micro-beads were moving at a 42-degree angle with respect to the bottom image axis (data not shown). This finding indicates that the ultrasound pulse was propagating at this angle along the xy-plane (as labeled in Fig. 1).

Neuronal cell culturing protocol

Our investigation on ultrasound-neuron interactions was performed with the Neuro-2a (N2a) mouse neuroblastoma cell line that is frequently used as an *in vitro* model system to study neurite outgrowth and its associated cytoplasmic signaling cascades (Wu et al. 1998). Differentiated N2a cells are known to exhibit morphological and bioelectrical characteristics similar to those of mature neurons, and they are therefore suitable for this investigation. In our experiments, undifferentiated N2a precursor cells were first cultured using Roswell Park Memorial Institute (RPMI) 1640 medium (R8758; Sigma-Aldrich, St. Louis, MO, USA) with 10% fetal bovine serum supplements (30–2020; American Type Culture Collection, Manassas, VA, USA). They were allowed to grow to 70% confluence inside a 37°C incubator (with 5% carbon dioxide), after which they were washed three times using phosphate-buffered saline and were trypsinized. Subsequently, the cells were seeded in a polystyrene dish at a density of 10^6 cells/dish.

To foster their differentiation into neuronal-like cells, the N2a cells at 24 h after seeding were cultured with a differentiation medium that consists of an RPMI 1640 solution with 10 mM retinoic acid (R-2625; Sigma-Aldrich, St. Louis, MO, USA) and 0.5% fetal bovine serum. During this phase, the cells were kept in a dark environment because retinoic acid is known to be sensitive to light. The differentiation process was allowed to take place for 24 h, during which approximately 70% of the cells underwent neuritogenesis (consistent with established observations; Wu et al. 1998). Afterward, the medium in the cell dish was changed to a buffer solution containing 145 mM NaCl, 5 mM KCl, 2 mM $CaCl_2$, 1 mM $MgCl_2$, 20 mM HEPES (4-[2-hydroxyethyl]-1-piperazineethanesulfonic acid), and 10 mM glucose (pH 7.4). The cell dish was then placed onto our ultrasound exposure platform to conduct experiment (working volume, 80 mL).

Analysis of ultrasound-induced neuronal morphology changes

The microscope video dataset corresponding to each experimental trial was analyzed offline by identifying instances of neuronal morphology changes such as neurite retraction and outgrowth, as well as cell body shrinkage and displacement. This identification was performed by manually examining the cell morphology in between image frames during and after ultrasound exposure. To quantify the extent of morphological changes, we have determined the percentage of neurite-bearing neuronal cells that underwent neurite retraction as a result of ultrasound exposure (this measure was chosen because it is a more apparent morphological change). Our classification criterion was based on whether the neurite tip of a neurite-bearing neuronal cell had displaced toward the parent cell body by more than 5 μm. Each analysis group comprised 250 cells, and this was repeated for four different cell groups ($N = 4$). To maintain data consistency, neurite-free neuronal cells were excluded from this quantitative analysis. The results for each acoustic setting were then compiled, and the presence of statistically significant difference was evaluated with the one-way analysis of variance (ANOVA) test (using 95% confidence interval). To determine whether the amount of neurite retraction was different between a pair of

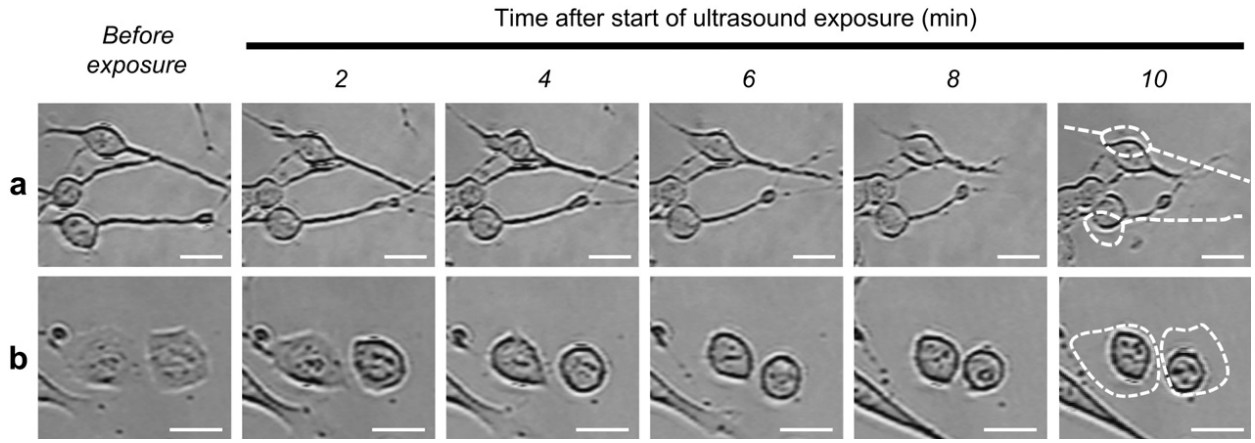

Fig. 3. Single-cell images showing changes in neuronal morphology over the course of 10 min of pulsed ultrasound exposure (1.168 W/cm^2 SPTA intensity: based on 0.84 MPa peak acoustic pressure, 100-cycle PD, 500 Hz PRF). (a) Neurite retraction and rounding of cell body for neurite-bearing neuronal cells (in the image after 10 min of exposure, dashed lines indicate original cell morphology). (b) A similar ultrasound-induced cell body shrinkage phenomenon for neurite-free neuronal cells. Scale bar = 20 μm.

acoustic exposure settings, a Tukey *post hoc* analysis was also performed in addition to ANOVA.

Experiments for mechanism analysis

Blockage of stretch-activated ion channels. To gain insight into the cellular mechanism behind ultrasound-neuron interactions, we have conducted an experiment with differentiated N2a cells whose stretch-activated ion channel activities were inhibited by gadolinium-III ions (Gd^{3+}). For these cells, their post-differentiation buffer medium included 10 or 50 μM gadolinium chloride hexahydrate (203289; Sigma-Aldrich) to facilitate ion-channel inhibition. Note that the Gd^{3+} supplements were added 10 min before the ultrasound exposure commenced.

Depletion of extracellular calcium ions. To determine whether calcium ions (Ca^{2+}) are involved in mediating ultrasound-neuron interactions, we have performed another experiment in which extracellular Ca^{2+} was depleted. In these experiments, $CaCl_2$ was excluded from the post-differentiation buffer medium (substituted with equivalent amount of $MgCl_2$). In addition, 5 mM EGTA (ethylene glycol tetra-acetic acid; E-3889, Sigma-Aldrich) was added to the buffer solution to chelate the remaining Ca^{2+} in the extracellular environment because of intrinsic ion transport out of the neuronal cells. The chelation reaction was allowed to take place for 5 min before exposure began.

RESULTS

Morphological changes in neurite-bearing and neurite-free neuronal cells

Our results generally showed that ultrasound can progressively reshape neuronal cell morphology over the course of exposure. For neurite-bearing neuronal cells (~70% of cells in the field of view), some of their neuritic processes were found to retract in response to ultrasound. Figure 3a shows an example of this observation for bipolar (two-neurite bearing) neuronal cells that received a 10-min ultrasound exposure at an SPTA intensity of 1.168 W/cm^2 (based on 0.84 MPa peak acoustic pressure, 100-cycle PD, 500-Hz PRF). As can be observed, the neuronal cells gradually withdrew one or more of their neurites over the exposure period. In addition, the neuronal cell bodies had shrunk with respect to the pre-exposure morphology. These results show that pulsed ultrasound is capable of instigating repulsive changes in neuronal morphology *in vitro*.

Ultrasound-induced cell body shrinkage was also observed in developing neuronal cells that had not undergone neuritogenesis (~30% of cells in the field of view). A two-cell image example corresponding to such an observation is provided in Figure 3b. It can be noted that, at the start of ultrasound exposure, these two neurite-free N2a cells exhibited a flattened cell body, although they had already been biochemically stimulated to differentiate into neuronal cells during pre-exposure culturing. As ultrasound exposure is applied, rounding of the cell body can be observed, and their cell boundary had retracted to a significantly smaller area compared with the pre-exposure morphology. It is worth noting that the SPTA intensity (1.168 W/cm^2) used to obtain these findings was slightly greater than the emission limit of 720 mW/cm^2 established for clinical diagnosis (Duck 2007). Despite this result, based on our mechanism analysis (see later in this section), the neuronal morphology changes observed here are unlikely to be induced thermally.

Morphological effects on a cluster of neuronal cells

As an extension of the previous observations, Supplementary Video 1 provides a time-lapse cineloop showing how a group of neuronal cells can change their morphology as a result of exposure to incremental levels of ultrasound (three intensity steps: 0.028, 0.266 and 1.168 W/cm^2). Note that the image frames were acquired at a 0.1 fps frame rate (played back at 10 fps), and the exposure duration was 10 min for each ultrasound level (*i.e.*, the cineloop covered a duration of 40 min). This cineloop illustrates that, when the intensity is increased to 1.168 W/cm^2, not only was the morphology of many neuronal cells modified by ultrasound, the overall appearance of the neuronal cell cluster was also significantly changed as a consequence.

To provide further insight, Figure 4 shows a schematic analysis of the morphological appearance of a neuronal cell cluster after 10 min of ultrasound exposure at SPTA intensities of 0.266 and 1.168 W/cm^2 (applied to the same cell group in sequence similar to that in Supplementary Movie 1). For the case with 0.266 W/cm^2 intensity (end-of-exposure morphology shown in Fig. 4b), occasional instances of neurite retraction and cell body displacement can be observed as depicted in Figure 4d by white and black arrows, respectively. The morphological response is significantly more drastic when the intensity is increased to 1.168 W/cm^2 (see Fig. 4c and 4e for end-of-exposure morphology and schematic analysis). This finding shows that the acoustic intensity is a physical parameter that influences the extent of the morphological effect exerted by ultrasound on neuronal cells.

Extent of morphological effect: dependent on acoustic intensity and peak acoustic pressure

As a quantitative analysis of the intensity dependence trend, Figure 5a plots the percentage of neurite-bearing neuronal cells with neurite retraction as a function of acoustic intensity (analysis was conducted on four independent cell groups for each intensity; $N = 4$). Of particular note is that, for the case with 1.168 W/cm^2 intensity, almost all neurite-bearing neuronal cells had retracted their neurites (one or more) over the ultrasound exposure period. This finding is in line with the schematic analysis shown in Figure 4e.

For a given intensity level, peak acoustic pressure was found to be a stronger contributing factor to ultrasound-induced neuronal morphology changes as compared with PD and PRF. As shown in Figure 5b, which plots the percentage of cells with neurite retraction for three parameter combinations, the use of a higher peak acoustic pressure (right column) yielded significantly more instances of neurite retraction (>30%) than the use of higher PRF (left column) or longer PD (middle column). In this case, the SPTA intensity for the higher-pressure configuration (0.234 W/cm^2) was lower than that of the other two (0.266 W/cm^2), thereby exemplifying the significant role that peak acoustic pressure plays in inducing neurite retraction. On the other hand, PD seems to assume a supplementary role in the process; if a longer duration is used in conjunction with a higher pressure (effectively yielding a higher SPTA intensity), more instances of neurite retraction would be generated. This observation is illustrated by comparing the right column of Figure 5a (for 100-cycle PD) against the right column of Figure 5b (for 20-cycle PD).

Post-exposure neurite growth can be observed

Following the end of ultrasound exposure, neuronal cells were found to exhibit growth behavior. For the same bipolar neuronal cells shown in Figure 3a, Figure 6a shows a series of images on the cells' post-exposure morphology. As noted earlier, the neurites of these cells were found to have retracted significantly by the end of ultrasound exposure. In the following 100 min, the neurites were found to have re-grown and recovered to neurite lengths similar to those before exposure. It is worth noting that the post-exposure neurite direction was slightly deviated from the original (see the pre-exposure image in Fig. 3a). This finding indicates that neurite growth direction can be modified by ultrasound exposure, and it could be the result of the perturbed cytomechanical force balance brought about by instances of neurite retraction (Ayali 2010).

For neurite-free neuronal cells, post-exposure outgrowth of neurite branches can be observed and is demonstrated in Figure 6b for two of these cells that appeared as a flattened entity before exposure and notably shrank during exposure (*i.e.*, same as those observed in Fig. 3b). Their morphology 100 min after the end of exposure showed sprouting of new neuritic processes from the cell body. As a result, ultrasound seems to have fostered post-exposure neuritogenesis in these neuronal cells.

Cellular mechanism: involves stretch-activated ion channels and Ca^{2+} messenger ions

For the ultrasound-induced neuronal morphological effect observed in Figures 3–6, stretch-activated ion channels and Ca^{2+} messenger ions were found to be involved in facilitating these effects. In particular, as shown in Figure 7, when Gd^{3+} (a known blocker of stretch-activated ion channel activities) was added to the medium, neurite retraction was largely suppressed in neurite-bearing neuronal cells during ultrasound exposure (administered using the same acoustic parameters as those for Fig. 3). This result is dependent on Gd^{3+}

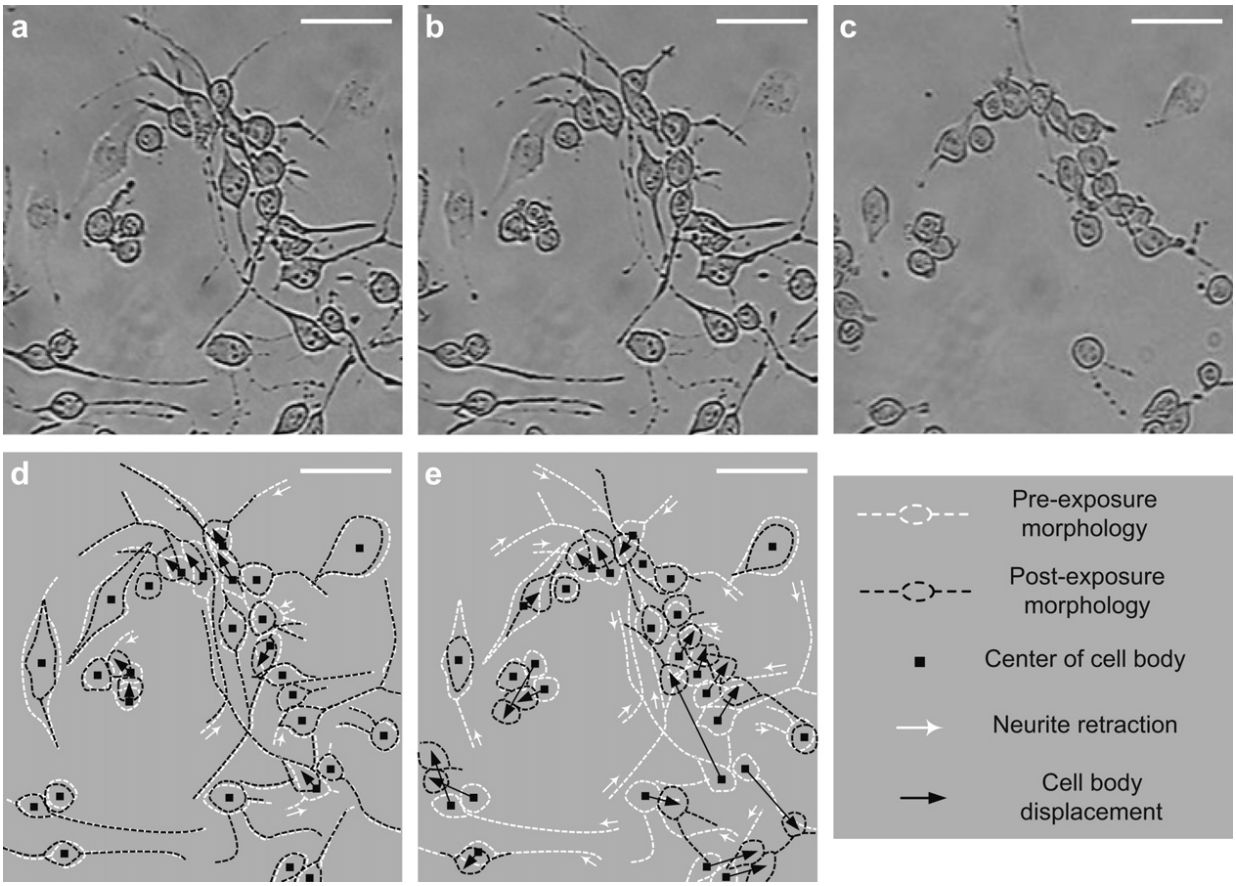

Fig. 4. Ultrasound-induced changes in the morphological appearance of a neuronal cell cluster. For the pre-exposure appearance shown in (a), the post-exposure appearance is shown in (b) after 10 min exposure at 0.266 W/cm^2 intensity (for 100-cycle PD, 500 Hz PRF, and 0.40 MPa peak acoustic pressure). Upon increasing the intensity to 1.168 W/cm^2 (by increasing peak pressure to 0.84 MPa), the same cell group showed additional changes as shown in (c) after 10 min of exposure. (d and e) Schematic analysis comparing the morphological changes between (a) to (b) and (b) to (c), respectively. White and black dashed lines denote the pre- and post-exposure neuronal cell morphology, respectively; instances of neurite retraction and cell body displacement are respectively indicated by white and black arrows. Scale bar = 100 μm.

concentration; for example, ultrasound was unable to induce neurite retraction in the presence of 50 μM Gd^{3+}, whereas some effects can still be observed at a concentration of 10 μM. Likewise, when extracellular Ca^{2+} was depleted (realized using a calcium-free buffer solution and chelation with EGTA), an inhibitory effect was also observed (Fig. 7), likely because of the lack of Ca^{2+} influx into the neuronal cell in response to ultrasound exposure. These findings provide initial insight into the cellular mechanism behind ultrasound-neuron interactions and are similar to the ones observed previously in mechanical intervention of neurite growth dynamics (Franze et al. 2009). These findings also indicate that ultrasound-induced neuronal morphological changes as observed in this study are unlikely to be attributed to thermal mechanisms, which still would have induced morphological changes even when stretch-activated ion channels were blocked by Gd^{3+}; however, this was not observed.

DISCUSSION

Using ultrasound to modify neuronal development dynamics is a novel concept that has not been explored in depth. In this work, we have demonstrated the feasibility of realizing such a concept *in vitro*. In particular, we have shown that pulsed ultrasound exposure over a certain period (10 min in our studies) can bring about neuronal morphological changes, including neurite retraction and cell body shrinkage (Fig. 3), and they might lead to instances of cell body displacement (Fig. 4 and Supplementary Movie 1). One potential explanation for these observations is that ultrasound-induced neurite retraction has likely disrupted the force balance of neuronal cells, and this in turn triggered physical migration of their cell body (Ayali 2010; Hanein et al. 2011). Note that the extent of such a bio-effect is dependent on the ultrasound intensity, with peak acoustic pressure being a major contributing factor in the process (Fig. 5).

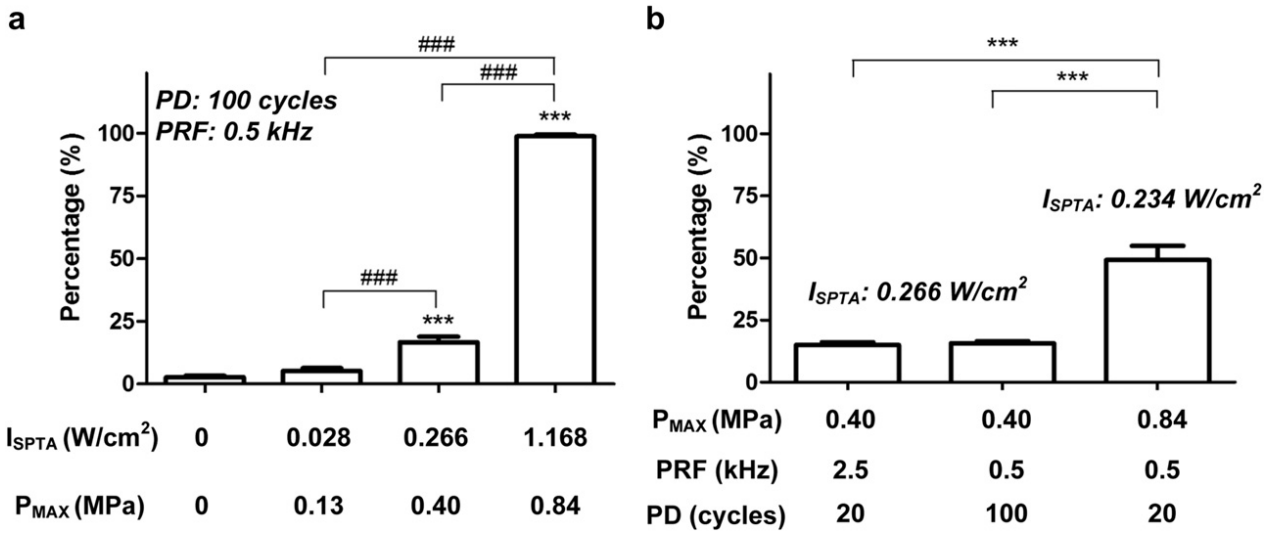

Fig. 5. Percentage of neurite-bearing neuronal cells that experienced neurite retraction as a function of (a) I_{SPTA} (for 100-cycle PD, 500 Hz PRF, 10-min exposure period) and (b) different combinations of P_{max}, PD, and PRF. Each statistical sample was obtained from an ensemble of 250 cells and was repeated over four different ensembles ($N = 4$). Error bars indicate standard error of mean; *** and ### indicate $p < 0.001$ with reference to sham control and in between exposure groups, respectively.

It is worth emphasizing that the repressive morphological effect induced by ultrasound on developing neuronal cells is transient in nature. Indeed, we have observed post-exposure neurite growth in neurite-bearing neuronal cells and neuritogenesis in neurite-free neuronal cells over a 100-min period (Fig. 6). This observation might be connected to the ultrasound-induced cell body shrinkage phenomenon, because cell shape decrease is known to reduce cytoskeletal contractility and tension (Wozniak and Chen 2009) that would in turn favor neurite formation (Da Silva and Dotti 2002). As such, ultrasound could have a stimulatory influence on neuronal growth dynamics, although it is acting as a repulsive cue during exposure. This conclusion is in agreement with a recent study that demonstrated how daily exposure to ultrasound can enhance neurite elongation in developing neuronal cells (Ren et al. 2010).

In terms of the biophysical mechanism responsible for ultrasound-induced neuronal morphological changes, our results have shown that mechanotransduction is likely to be involved, as blockage of stretch-activated ion channels has led to significant suppression of ultrasound-induced morphological changes (Fig. 7). In addition, Ca^{2+} messenger ions seem to have an important role in the transduction

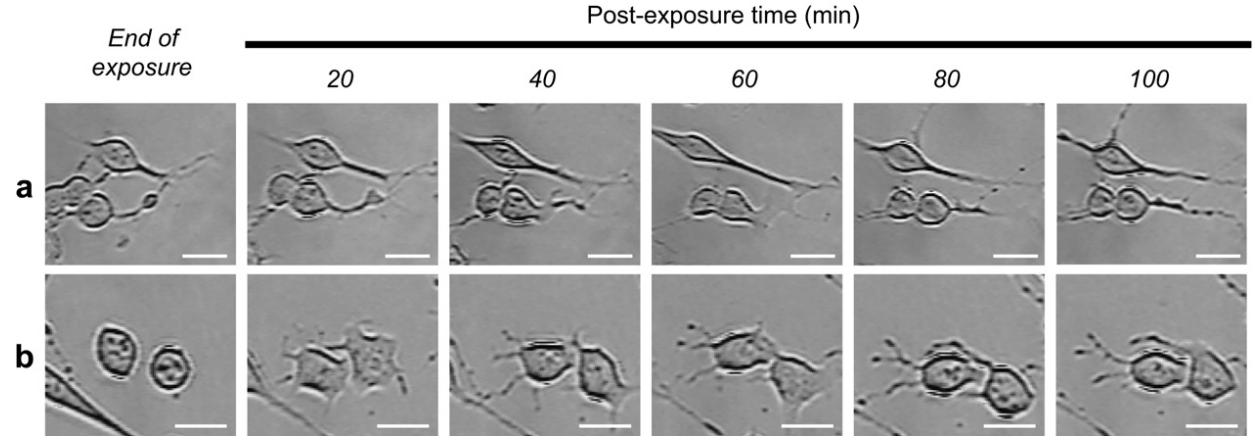

Fig. 6. Neurite regrowth and outgrowth in neuronal cells after the end of 10 min of pulsed ultrasound exposure (for the same cells shown in Fig. 2). (a) For cells with existing neurites, they showed significant neurite regrowth after exposure. (b) For cells that did not undergo neuritogenesis prior to exposure, they showed post-exposure sprouting of new neurite branches over a 100-min period after experiencing ultrasound-induced cell body shrinkage. Scale bar = 20 μm.

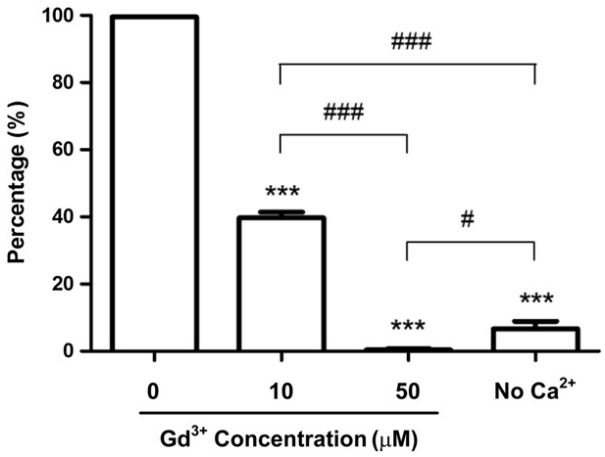

Fig. 7. Reduction in the percentage of neuronal cells with ultrasound-induced neurite retraction after blockage of stretch-activated ion channel activities using Gd^{3+} or depletion of extracellular Ca^{2+} using EGTA. Results were obtained with these exposure parameters: 1.168 W/cm^2 SPTA intensity; 0.84 MPa peak acoustic pressure; 100-cycle PD; 500 Hz PRF; 5-min duration. Error bars indicate standard error of mean ($N = 4$, each taken from average of 250 cells with existing neurites); ***$p < 0.001$ with respect to normal exposure results (left column); #$p < 0.05$ and ### $p < 0.001$ between two treatment groups.

process, because depletion of extracellular Ca^{2+} has resulted in similar inhibition of bioeffects (Fig. 7). Therefore, ultrasound might essentially be acting on neuronal cells in ways similar to mechanical stress (Franze et al. 2009); this is possible because ultrasound is known to exert radiation force along its path as a linear function of intensity (Dalecki 2004; Ahmadi et al. 2012). Indeed, such an acoustic radiation force effect has been observed during our acoustic field calibration in which ultrasound-induced micro-bead displacements were observed over the microscope's field of view (see the Acoustic Field Calibration subsection). As a result, ultrasound could be operating as a non-contact form of mechanical stimulation similar to the case of ultrasound-enhanced bone formation (Perry et al. 2009).

Given that our findings have demonstrated the potential role of ultrasound in modulating neuronal development, it would be interesting to unravel further details on the downstream bioeffects that may be elicited. For example, one aspect to be investigated further is the causal relationship between post-exposure neurite outgrowth observed in this work and the cytoplasmic signals associated with neuronal development, such as the Rho proteins that are important for cytoskeleton regulation (Govek et al. 2005). Ideally this investigation would involve the use of cellular fluorescence imaging techniques to explore space-time signaling dynamics (Pertz 2010). A related investigation that should be pursued in parallel is to conduct a neurotrophic factor expression assay on ultrasound-treated neuronal cells. These studies would help to correlate our current findings with previous reports that showed ultrasound-induced enhancement of neurotrophic factors *in vivo* (Chang and Hsu 2004; Chen et al. 2010; Crisci and Ferreira 2002).

CONCLUSION

This work is perhaps the first demonstration that ultrasound can modulate neuronal development *in vitro* through triggering temporary neurite retraction and inducing cell body shrinkage. From a therapeutic standpoint, the reported findings should be of interest because they showed that ultrasound could possibly serve as a transient repulsive cue for modifying the physical positioning and cytomechanical characteristics of developing neurons. As such, ultrasound might have potential in facilitating the remodeling of neuronal development processes. From a biophysical perspective, it is important to investigate further how ultrasound modulates neuronal development dynamics by examining subcellular level events, such as transmembrane ion fluxes and cytoplasmic signaling changes. Such analysis would help to unravel additional details on ultrasound-neuron interactions, and in turn provide stronger mechanistic foundations for further developments on this topic.

Acknowledgments—The authors thank Dr. Wai Hung Sit for his technical assistance with cell culturing. This work was supported in part by the Hong Kong Innovation and Technology Fund (ITS/292/11).

SUPPLEMENTAL DATA

Supplementary data related to this article can be found online at http://dx.doi.org/10.1016/j.ultrasmedbio.2012.12.003.

REFERENCES

Ahmadi F, McLoughlin IV, Chauhan S, ter Haar G. Bio-effects and safety of low-intensity, low-frequency ultrasonic exposure. Prog Biophys Mol Biol 2012;108:119–138.

Arimura N, Kaibuchi K. Neuronal polarity: from extracellular signals to intracellular mechaisms. Nat Rev Neurosci 2007;8:194–205.

Ayali A. The function of mechanical tension in neuronal and network development. Integr Biol 2010;2:178–182.

Bystritsky A, Korb AS, Douglas PK, Cohen MS, Melega WP, Mulgaonkar AP, DeSalles A, Min BK, Yoo SS. A review of low-intensity focused ultrasound pulsation. Brain Stim 2011;4:125–136.

Chang CJ, Hsu SH. The effects of low-intensity ultrasound on peripheral nerve regeneration in poly(dl-lactic acid-co-glycolic acid) conduits seeded with Schwann cells. Ultrasound Med Biol 2004;30:1079–1084.

Chen WZ, Qiao H, Zhou W, Wu J, Wang ZB. Upgraded nerve growth factor expression induced by low-intesnity continuous-wave ultrasound accelerates regeneration of neurotometicly injured sciatic nerve in rats. Ultrasound Med Biol 2010;36:1109–1117.

Crisci AR, Ferriera AL. Low-intensity pulsed ultrasound accelerates the regeneration of the sciatic nerve after neurotomy in rats. Ultrasound Med Biol 2002;28:1335–1441.

Dalecki D. Mechanical bioeffects of ultrasound. Annu Rev Biomed Eng 2004;6:229–248.

Da Silva JS, Dotti CG. Breaking the neuronal sphere: Regulation of the actin cytoskeleton in neuritogenesis. Nat Rev Neurosci 2002;3: 694–704.

Duck FA. Medical and non-medical protection standards for ultrasound and infrasound. Prog Biophys Mol Biol 2007;93:176–191.

Ehrlicher A, Betz T, Stuhrmann B, Koch D, Milner V, Raizen MG, Kas J. Guiding neuronal growth with light. Proc Nat Acad Sci 2002;99: 16024–16028.

Franze K, Gerdelmann J, Weick M, Betz T, Pawlizak S, Lakadamyali M, Bayer J, Rillich K, Gogler M, Lu YB, Reichenbach A, Janmey P, Kas J. Neurite branch retraction is caused by a threshold-dependent mechanical impact. Biophys J 2009;97:1883–1890.

Franze K, Guck J. The biophysics of neuronal growth. Rep Prog Phys 2010;73:094601.

Goldberg JL. Intrinsic neuronal regulation of axon and dendite growth. Curr Opin Neurobiol 2004;14:551–557.

Govek EE, Newey SE, van Aelst L. The role of the Rho GTPases in neuronal development. Gene Dev 2005;19:1–49.

Guan KL, Rao Y. Signaling mechanisms mediating neurnal reponses to guidance cues. Nat Rev Neurosci 2003;4:941–956.

Halliwell M. A tutorial on ultrasound physics and imaging techniques. Proc Inst Mech Eng H 2010;224:127–142.

Hanein Y, Tadmor O, Anava S, Ayali A. Neuronal soma migration is determined by neurite tension. Neuroscience 2011;172:572–579.

Hoffman-Kim D, Mitchel JA, Bellamkonda RV. Topography, cell repsonse, and nerve regeneration. Annu Rev Biomed Eng 2010;12: 203–231.

Ming GL, Henley J, Tessier-Lavigne M, Song HJ, Poo MM. Electrical activity modulates growth cone guidance by diffusible factors. Neuron 2001;29:441–452.

Norman LL, Stroka K, Aranda-Espinoza H. Guiding axons in the central nervous system: a tissue engineering approach. Tissue Eng Part B Rev 2008;14:33–51.

Perry MJ, Parry LK, Burton VJ, Gheduzzi S, Beresford JN, Humphrey VF, Skerry TM. Ultrasound mimics the effects of mechanical loading on bone formation in vivo on rat ulnae. Med Eng Phys 2009;31:42–47.

Pertz O. Spatial-temporal Rho GTPase signaling—where are we now? J Cell Sci 2010;123:1841–1850.

Ren C, Li JM, Lin X. LIPUS enhance elongation of neuritees in rat cortical neurons through inhibition of GSK-3β. Biomed Environ Sci 2010;23:244–249.

Rossi F, Sara Gianola S, Corvetti L. Regulation of intrinsic neuronal properties for axon growth and regeneration. Prog Neurobiol 2007;81:1–28.

Schmidt CE, Leach JB. Neural tissue engineering: strategies for repair and regeneration. Annu Rev Biomed Eng 2003;5:293–347.

Smith DH. Stretch growth of integrated axon tracts: extremes and exploitations. Prog Neurobiol 2009;89:231–239.

Song HJ, Poo MM. The cell biology of neuronal navigation. Nat Cell Biol 2001;3:E81–E88.

Suter DM, Miller KE. The emerging role of forces in axonal elongation. Prog Neurobiol 2011;94:91–101.

Tufail Y, Matyushov A, Baldwin N, Tauchmann ML, Georges J, Yoshihiro A, Tillery SIM, Tyler WJ. Transcranial pulsed ultrasound stimulates intact brain circuits. Neuron 2010;66:681–694.

Tufail Y, Yoshihiro A, Pati S, Li MM, Tyler WJ. Ultrasonic neuromodulation by brain stimulation with transcranial ultrasound. Nat Protoc 2011;6:1453–1470.

Tyler WJ, Tufail Y, Finsterwald M, Tauchmann ML, Olson EJ, Majestic C. Remote excitation of neuronal circuits using low-intensity, low-frequency ultrasound. PLoS ONE 2008;3:e3511.

van Ooyen A. Using theoretical models to analyse neural development. Nat Rev Neurosci 2011;12:311–326.

Wozniak MA, Chen CS. Mechanotransduction in development: A growing role for contractility. Nat Rev Mol Cell Biol 2009;10: 34–43.

Wu G, Fang Y, Lu ZH, Ledeen RW. Induction of axon-like and dendrite-like processes in neuroblastoma cells. J Neruocytol 1998; 27:1–14.